Millimeter-Wave Antenna Implementation for 5G Smartphones

Filipa Fernandes
Universidade de Lisboa
Instituto Superior Técnico
filipa.ss.fernandes@ist.utl.pt

***Abstract*—The upcoming 5G wireless technology is sparking a number of paradigm shifts in the mobile phone industry regarding antenna design and implementation. The transition to the mm-Wave band allows for unprecedented data transmission rates but, at the same time, opens the Pandora box of reliable communications using high frequencies.**

The present work assesses the implementation of mm-Wave antennas in 5G smartphones to minimize impairments caused by high frequencies, modern mobile phone form factor constrictions and dynamic environment characteristics. A general comparison process is established based on two mm-Wave antenna families, patches (PBS) and monopoles (MBS), at 39 GHz, to evaluate their potential and limitations when integrated into 5G smartphones.

This process comprises two stages: first, a coverage study, to assess how well distributed in space is the power radiated by the beam steering array; and second, an evaluation of the MIMO channel performance depending on the antenna family, polarization, environment scenario, and potential body blockage. The latter is done using a discrete geometrical MIMO channel simulator developed to recreate the mm-Wave propagation conditions in any scenario (from rural to urban). It includes the effects of real antennas, smartphone metallic chassis and user influence (body blockage and depolarization).

***Index Terms*—5G, Small antennas, Beamforming, MIMO, mm-Wave, Smartphones.**

I. Introduction

5G is the wireless technology being currently developed to sustain the high amounts of data rate, connections, bandwidth and low latency requirements that come with more users, devices, and ambitious endeavors such as Smart Cities or Autonomous Vehicles. However, the topic of 5G is still somewhat abstract when it comes to mm-Wave antenna technologies. Despite the existence of mm-Wave antennas in radio infrastructures being deployed in the near future, mm-Wave antenna technologies for 5G cellular handsets are still at their early stages. There is still no standardized method to design and implement these antennas in mobile phones due to the lack of knowledge on mm-Wave 5G wireless system benchmarks. This prevents the impact evaluation of design parameters such as user influence, handset effects, gain coverage and so on, since there is not a reference for comparison [1]. So far, some of the major challenges for mm-Wave antenna design and implementation have been identified and in the literature there are several proposed approaches to mitigate them.

The first obstacle is the drawback of using the mm-Wave band. These frequencies offer wider bandwidth, which is very appealing for large data rate transmissions. Unfortunately, their poor propagation conditions make it a difficult band to work with since there is strong path loss, atmospheric absorption, and low penetration through objects, as well as little diffraction around obstacles. To counteract this, most mm-Wave antennas are used in large arrays, so that the increased array gain can compensate for the huge losses. This is only viable because mm-Wave antennas are electrically small sized and fit better into tighter spaces such as the mobile phone. In [2] a pair of 16- element patch arrays is placed on the top and bottom of the phone. Meanwhile, [3] presents 8 modules of 8-element patch arrays distributed in the handset.

If the handset can accommodate more antennas, these can be grouped into arrays, enabling beam steering. Therefore, the regular MIMO approach used in mobile phones can be transformed into hybrid MIMO, which is a combination of regular spatial multiplexing (SM) MIMO with beamforming (BF) [4], [5]. Naturally, SM and BF can be used separately but, for specific situations, they are stronger together. According to [3], its BF modules are meant to transmit 8 separate data streams but, if any of the modules is blocked, the rest can abandon the MIMO approach and be used as normal BF modules to transmit a single data stream.

However, accommodating for a large number of antennas in a mobile phone is challenging. Nowadays, there is a lack of space for hardware in the handset [6]. These compact form factors, besides having to accommodate for other wireless technologies, need to integrate batteries, large screens, two cameras, fingerprint scanning, gyroscope, vibrator etc. to ensure that the user can have the best experience. This originated a lot of articles for compact and creative antenna solutions to optimize the space usage within the phone. In [4] a dual polarized antenna is used: two arrays are implemented in a phone with switchable polarization, reducing the number of arrays needed to half while doubling the spectral efficiency.

Another big challenge for the antenna design team is that most state of the art smartphones also have metallic casings. These serve an aesthetic purpose, while providing structural sturdiness and heat dissipation. However, these design choices place another hurdle for mm-Wave antenna placement, since bigger screens and metallic form factors increase the amount of metal in proximity with the antennas. For these high frequencies, metal is responsible for the radiation pattern's dramatic loss of shape. Therefore it is vital to include the form factor in the antenna behavior studies.

Besides these design constrictions, the user's influence in the

antenna behavior must be considered. It manifests in two ways: first, the human body causes antenna impedance mismatch and behaves like an absorber and a reflector for mm-Waves, blocking any signal that comes in its direction. In [7] tests were made at 15 GHz to shows that the body is a clear obstacle to signal propagation [8]. A hand/head close to the phone will have major disturbances in the antennas radiation pattern and must be accounted for in test simulations. This is why having many antenna arrays in the phone is very important. If the user is blocking a certain antenna array with his hand the communications can still be carried out by the remaining arrays; second, it is hard to predict how the user will position the handset in relation to the BS. This can ruin the polarization alignment between the user equipment (UE) and the BS, which will surely deteriorate the MIMO performance. Ultimately, this would render solutions such as the dual polarized antennas useless.

Since this is a novel subject still under investigation, there are not too many articles in the literature that rigorously account for all these design and implementation requirements. This stems from the fact that there are still some testing limitations for the experimental assessment of 5G MIMO. Often, not every test scenario can be carried out, either because it is too expensive, complex or because there is a lack of resources to conduct them all. If the amount of real life test scenarios is limited, it is difficult to take any generalized conclusions out of it.

The communication channel takes a big part in determining the MIMO system performance. Therefore, it is wiser to first establish an accurate and reliable channel model that recreates the environment and propagation features of mm-Wave, while incorporating all the antenna aforementioned design parameters [9]. Some of these models already exist, like [10] but they resort to simplifications regarding antenna modeling and don't take some of the discussed design parameters into consideration (smartphone chassis or the user influence).

Ultimately, the design difficulties mentioned above might make the prediction of the antenna's radiation pattern very challenging for mm-Waves. The ideal narrow beams obtained in free space for MIMO and beamforming might lose their shape when realistic environment conditions come into play (like the phone chassis or the user's influence). If realistic radiation pattern prediction is not a reliable option, then basing an antenna's design in achieving a specific beam behavior will be a vain effort.

Patch based solutions, PBS, are very popular in the current literature. Their low profile, and high gain values when used in an array configuration suggest that the PBS antenna is a good candidate for 5G smartphone implementation. Not to mentioned its dual polarization ability. However, instead of focusing solely on gain, it is worth analyzing also the average coverage. A good option would be for an antenna that is able to radiate power in more directions, such as monopole based solutions, MBS. These are also smaller, so they would not interfere too much with the legacy antennas, and are less complex to produce and easier to implement in the handset. These are the two antenna solutions being evaluated in this work. The goal is to identify which one is best suited for smartphone implementation based off swept coverage area and MIMO channel performance and considering all the design and implementation restrictions enumerated above.

II. Antenna Array Design

The antenna solutions were designed as linear four element arrays in the 3D electromagnetic solver CST Microwave Studio. They were tuned for 39 GHz. As a rule of thumb for 5G, the requirement is that the antenna's reflection coefficient is below -10 dB. In this project, instead of using circuitry, the impedance match was assured through manipulation of the antenna's electrical parameters. The number of antenna elements for the linear array was picked so that the beams had enough gain but not be too narrow to the point of affecting coverage. If the array is too small, the array gain may not cover the propagations losses induced by mm-Wave. Also, larger arrays require higher phase shifter power consumption and time overhead to steer the array beam, which reduces the smartphone's battery autonomy. A $N = 4$ linear array's size resulted as a compromise.

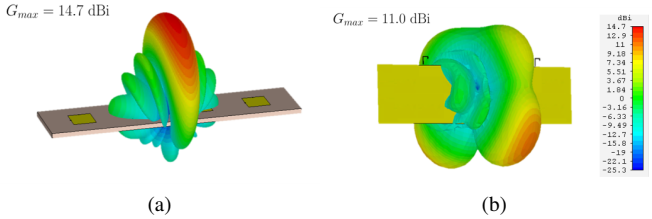

(a) (b)

Fig. 1. Antenna array radiation patterns for $\psi = 90^o$; a) PBS; b) MBS.

The PBS antenna is composed of a squared ground plane with a 0.5 mm thick Rogers RT 5880 substrate (loss tangent of 0.0004), and a 2.43×2.43 mm patch. The metallic ground and patch are made of copper with an electrical conductivity of $5.95 \times 10^7 Sm^{-1}$. It adopts a probe feeding approach in CST with discrete ports. Since it is a dual polarized antenna, two feeding pins are placed orthogonally to provide a polarization along the y-axis and another along the x-axis. The PBS antenna was used in a 6.09×24.5 mm linear array configuration with four elements, as seen in Figure 1a). This same radiation pattern is exhibited in Figure 2 with addition of the θ, φ and ψ angles for coordinate definition.

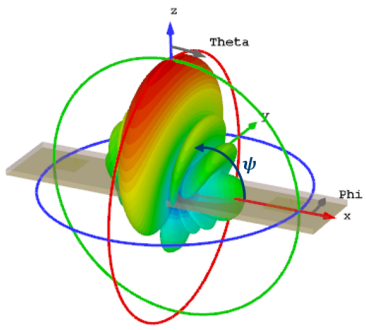

Fig. 2. Radiation pattern for a linear, four element PBS array for beam $\psi = 90^o$ to indicate the angles θ, φ and ψ.

The angle θ is defined by the z axis and the vector from the origin to the observation point P, varying from 0 to 180^o. The angle φ is defined by x and the projection of P in the xy plane from 0 to 360^o. The angle ψ identifies the beam steering notation based on the radiation pattern's inclination. It is measured as the angle between the array's axis to the beam's main lobe. Therefore Figure 1a) shows the PBS's $\psi = 90^o$ beam. The spacing between antenna elements, 0.7λ, was determined not only by the desired gain (maximum gain of 14.7 dBi) but also by the need to provide a good isolation between adjacent elements ($s_{ij} < -10$ dB).

The MBS antenna model is a folded 1.4×1.75 mm monopole, which is considerably smaller than the PBS. It is made out of the same copper material as the patch. The MBS's ground plane dimensions vary, since this solution will use the mobile phone as a ground plane. It is also used as a linear array with four antenna elements and a 0.7λ spacing, displayed in Figure 1b) that shows the radiation pattern for the $\psi = 90^o$, with an 11.0 dBi maximum gain value.

III. Influencing Factors on the Antennas' Behavior

A. Form Factor

The smartphone form factor used for CST simulations models a phablet developed by Intel, portrayed in Figure 3. This model is mostly a compact structure made out of copper. The form factor has a hollow volume in the bottom, where a FR- 4 substrate ($\varepsilon_r = 4.5$, $tan\delta = 0.025$) was placed, to accommodate the antennas. The bottom area of the phone is encapsulated by a plastic casing, marked in blue ($\varepsilon_r = 2.8$, $tan\delta = 0.0009$). This space is partially occupied by the sub 6-GHz legacy antennas that were loaded with a 50 Ω impedance in the simulation model, so that their effect would still be accounted for without them being active (since the working frequency bandwidth is different).

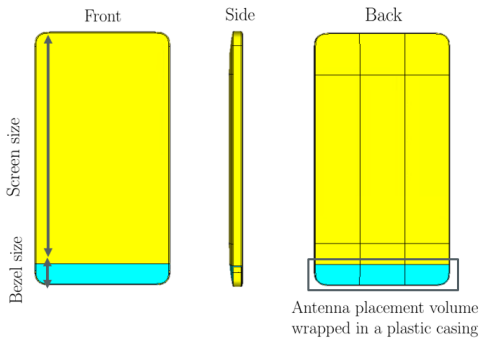

Fig. 3. Mobile phone form factor with front, side and back view.

The PBS array was integrated in the bottom half of the phone's back, in the volume reserved for the antennas, as seen in Figure 4a). The MBS was also implemented in the same antenna volume, on top of the phone's dielectric, using the phone as a ground plane, as can be seen in Figure 4b).

It is evident that the radiation patterns suffer some changes by comparing Figure 5 to Figure 1. This is due to the fact that

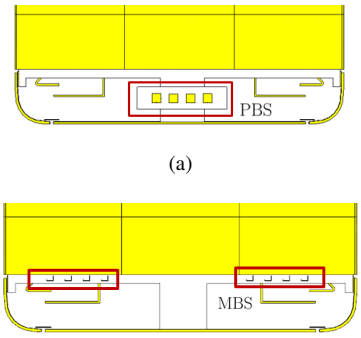

Fig. 4. Array implementation in the mobile phone's form factor; a) PBS; b) MBS.

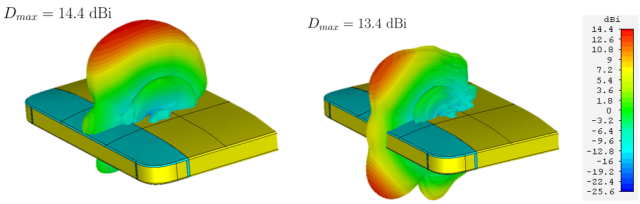

Fig. 5. Antenna array radiation patterns for $\psi = 90^o$ with form factor integration; a) PBS; b) MBS.

the phone's chassis that encapsulates the antennas is made of metal. Also, both antenna families have similar maximum gains now, with a small difference of around 1 dB. To study the influence of the mobile phone components on the antenna's radiation pattern behavior, some alterations were made to the original form factor. Gorilla 5 screen glass [11] ($\varepsilon_r = 6.96$, $tan\delta = 0.014$) was added to the front of the phone and the plastic casing was prolonged all through the back of the phone, to replace the yellow metal rear case. Also, the phone's bezel size was altered. The bezel size is the area of the display surrounding the screen. If it decreases to accommodate a bigger screen, it takes space away from the antenna placement volume by covering it with metal. Thus, the bezel size was reduced from it's original 14.6 mm to 2.23 mm, in onrder to recreate the Iphone X or the Samsung S9 bezel sizes.

The first two modifications to the form factor did not cause any significant changes to the antennas' radiation patterns. However, the bezel size study confirmed that the addition of metal is detrimental to the propagation of the electromagnetic fields at mm-Wave frequencies, as can be seen from Figure 6. Since changing the form factor size required more metal solely in the front of the phone, the PBS was not severely affected, as represented in Figure 6a), since it is radiates towards the back of the phone. For the MBS, however, the lobe that was directed towards the front of the phone was completely suppressed as seen in Figure 6b).

However, this issue is solvable, since there are multiple other repositioning options for both the PBS and the MBS to avoid the blockage. From this analysis, it is clear that the most important smartphone material to consider when

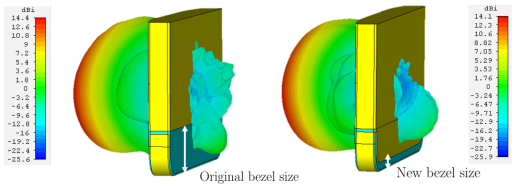

(a)

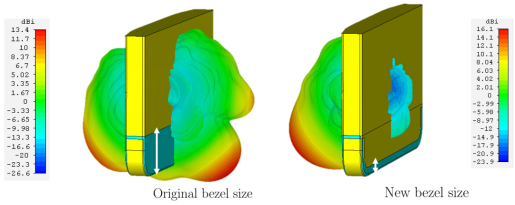

(b)

Fig. 6. Antenna array radiation patterns for $\psi = 90^o$ with altered bezel sizes; a) PBS; b) MBS.

studying its influence on the antenna's behavior is, in fact, the smartphone's metal chassis. The influence of the other form factor materials was minimal, suggesting that these are less relevant for the study, since they would only increase the computation time without affecting too much the results. The rest of the study will be carried out with the original form factor in Figure 3.

B. User's hand grip

A human hand was chosen to model the user's body effect in the performance of mm-Wave antennas implemented in a mobile phone. Intel provided a 3D computer-aided model (CAD) of a hand grip, from older projects performed in the sub-6 GHz spectrum. These models can be integrated into CST simulations and the grip posture can be adjusted to the phablet's dimensions. The hand grip used is commonly known as Talk Mode, TM, representing the way the phone is hold when making a phone call, as seen in Figure 7.

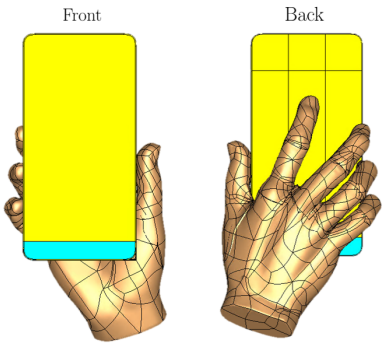

Fig. 7. Front and back view of the Talking mode hand grip.

Because this CAD model was designed for sub-6 GHz frequencies, its dielectric properties needed to be updated to mm-Wave frequencies. Although hands are an intricate part of the human body, with skin, bone, muscle and blood vessels, a simplification was adopted to make the model only out of muscle tissue. From all the materials considered (muscle, bone and skin), the muscle had the biggest influence in the results. It has the highest electrical conductivity out of all the hand components considered in [12] for 39 GHz, $42.5\ Sm^{-1}$, thus introducing a huge attenuation at mm-Wave frequencies and dominating the wave propagation behavior. Figure 8 and Figure 9 display the radiation patterns of the arrays implemented in a form factor with the hand grip included for two steering directions, $\psi = 90^o$ and $\psi = 70^o$.

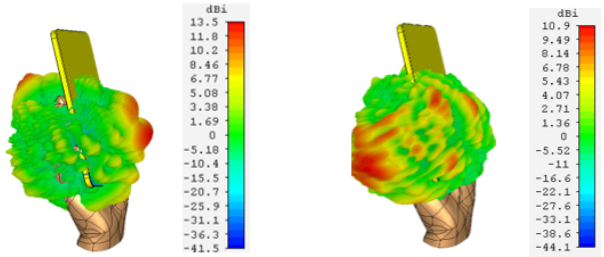

(a) (b)

Fig. 8. Antenna array radiation patterns for PBS integrated in the form factor with the TM hand grip; a) $\psi = 90^o$; b) $\psi = 70^o$.

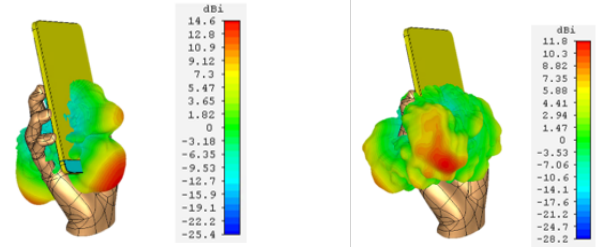

(a) (b)

Fig. 9. Antenna array radiation patterns for MBS integrated in the form factor with the TM hand grip; a) $\psi = 90^o$; b) $\psi = 70^o$.

It is clear that all radiation patterns suffer the same effects when in close proximity with the hand. The once narrow and directive beams now take a random and unpredictable shape for their radiation pattern. Considering the transition from the $\psi = 90^o$ beam to the $\psi = 70^o$ beam, it is noticeable that beam steering ability is also affected since all the beams lose shape when the user is involuntary covering the antennas, loosing its directivity.

This happens because of the human body's dielectric properties for the mm-Wave band that cause impedance mismatch, energy absorption (in the near-field) and propagation body shadowing (in the farfield). However, for such high frequencies, the electric field does not penetrate the human body too deeply (at epidermis level) and the energy gets absorbed in the near-field very quickly.

Figure 10 shows a representation of the E-fields propagation for the PBS over the phone and the user's hand for the TM

grip. A transversal cut to the hand + form factor confirms the expectations. In the place of the user's hand, a big dark blue area is apparent, entailing the lack of electric field penetration. It is either reflected in the user's hand or escaping from gaps in between the its fingers.

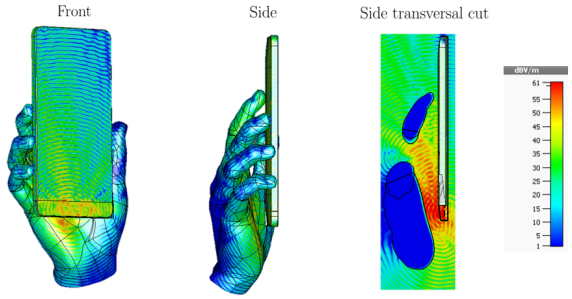

Fig. 10. E-fields propagation contour plots for the PBS array integrated into the form factor with the hand grip.

For this particular antenna positioning, the PBS is severely affected since it radiates through the back of the phone that is completely cupped by the user's grip. This is an unavoidable but recurrent challenge that mm-Wave propagation faces and must be diverted through resourceful techniques such as the process of beam switching or array switching.

IV. Coverage Study

Having high gain is not the sole argument to consider in mm-Wave antenna selection for 5G smartphone integration. There must be a balance between the array's coverage abilities and the value of gain provided. Highly directive beams require beam agility to maintain the link alignment and, consequently, its quality. Antenna arrays allow the process of beam steering, which means that one antenna array alone can provide multiple beams pointing into various directions. To achieve a compromise between gain and coverage, a fair assessment would be to quantify the area that a set of beams sweeps without forfeiting an acceptable maximum gain value. In other words, a percentage of coverage function is obtained to identify which of the antenna families provides the best swept coverage area, for a given threshold gain value, under which wireless communications are not viable.

A. Codebook development

The first step to this study is recreating, in a simulation, the beam sweep performed by the antenna arrays. This is achieved by computing the array's gain values for each beam in all (θ, φ) directions of observation.

In order to obtain the several ψ beams, a codebook must be developed. A codebook is a set of $M \times N$ weights that are applied to the N individual antennas of an array to generate M beams for different ψ values. For a specific ψ_m, out of the M available, these N-1 weights are defined as $a(m, n)$ and are computed trough linear array theory. Because these are linear and uniform arrays, each of the antenna elements will require a progressive phase shift of δ in its feeding, given by Equation 1, where k is the wave number and d is the spacing between antenna array elements.

$$\delta_{\psi_m} = -kd\cos\psi_m; \tag{1}$$

Given the real phase shifters' limitations, it is not possible to perform continuous beamsteering. It is a discrete process for specific ψ values, and, therefore, discrete values of δ phase.

CST has this functionality implemented in the post-processing tab, under the name of Combining tool. The $N-1$ values of δ must be typed in the feeding of the antennas of the simulation for one beam ψ to be generated. For a bigger dimension codebook, this can become a tedious and time consuming process, even with the help of a programmed macro.

In order to expedite the process, part of this work's efforts focused on developing a tool that makes the codebook generation and representation an automatic process. This tool is configurable, allowing the user to define parameters such as the dimension of the codebook, the phase shifter's resolution and displays gain coverage information. CST has an option for exporting the individual antennas' radiation pattern characteristics in the farfield region into ASCII file (containing not only the mutual influence between antenna elements but also the form factor and the user's influence).

The information from these individual files was used to develop this MATLAB tool called Antenna Pattern Analysis Toolbox (APA TBX), that, with a single simulation, generates and represents a set of beams similar to the ones that would be obtained with the Combining Tool from CST. Instead of calculating δ exteriorly and typing it into CST, all that is needed is a list of desired ψ values, working frequency and antenna element spacing in the array.

Using the APA TBX is quicker and it offers more freedom, since functionalities like bit resolution and phase quantization can be included. In this tool, a realistic phase shifter was implemented with a bit resolution limitation. For a phase shifter with B bits there are 2^B possible phase shifts that can be provided to the antennas. After the δ values are calculated for each ψ, the tool approximates them to the closest available phase shift. If the number of bits used is too small, this can lead to some small deviation from the original intended ψ that would be obtained in CST. However, this would resemble real life limitations in an user terminal more than CST does.

Figure 11a) shows the four CST individual radiation patterns for a linear MBS array with four elements (highlighted in the blue squares) in the mobile phone (suppressed for better visualization). Using the externally calculated δ values a steering beam of $\psi = 90^o$ was created in Figure 11 b) using CST's combining tool and. Figure 11 c) presents the same radiation pattern obtained with the developed Matlab tool.

This tool also allows for codebook envelope visualization. This is the term used to refer to the representation of the envelope of all discrete beams represented simultaneously. Figure 12a) and Figure 12b) shows the 3D representation of a 17-entry codebook envelope for, respectively, the PBS array and MBS arrays. This codebook envelope will be used

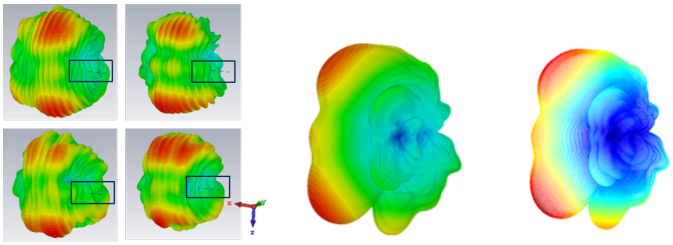

(a) (b) (c)

Fig. 11. Codebook development process for $\psi = 90^o$; a) CST b) APA TBX.

to construct the coverage function that the coverage study is based on.

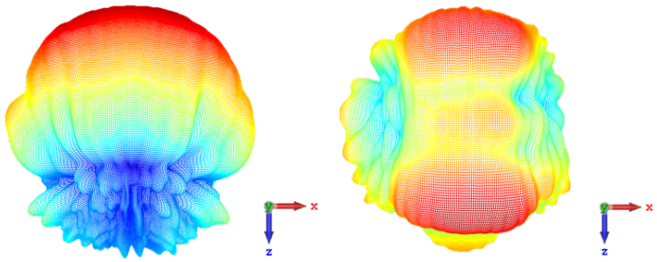

(a) (b)

Fig. 12. 3D 17-entry codebook envelope representation; a) PBS; b) MBS.

B. Coverage function

Consider a spherical representation of an antenna gain in the solid angle, as represented in Figure 13. The center corresponds to the minimum gain value of the radiation pattern, G_{min}, and the radius is the antenna's maximum gain, G_{max}. The 3D codebook envelope of the PBS array is delimited by the coverage sphere. Suppose that a certain gain threshold value is established, $G_{threshold}$, under which the gain is too low for the antenna to be used. The coverage function expresses the percentage of registered directions (θ,φ) of the codebook envelope that are within that gain interval, $G_{threshold} < G < G_{max}$. This percentage will quantify the full gain coverage potentiality of each antenna solution.

However, when exporting data for a radiation pattern, CST samples the data for equally spaced points of the radiation pattern in $\hat{\theta}$ and $\hat{\phi}$ directions. This creates a 180×360 grid, with uniformly distributed points for each direction. However, in spherical coordinates, this does not correspond to an uniform distribution of points over the sphere. The nodes become denser as θ approaches 0 or 180^o, and sparse when approaching 90^o as can be seen in Figure 14. This would mean that the percentage of points abiding the $G_{threshold} < G < G_{max}$ condition would be dependent on how the orientation of radiation pattern.

A weight function must be added to properly account the power density distribution in a polar grid from rectangular grid data.The weight function, pc_w, is given by Equation 2. Areas with higher point density will weight less than in areas where the points are sparser.

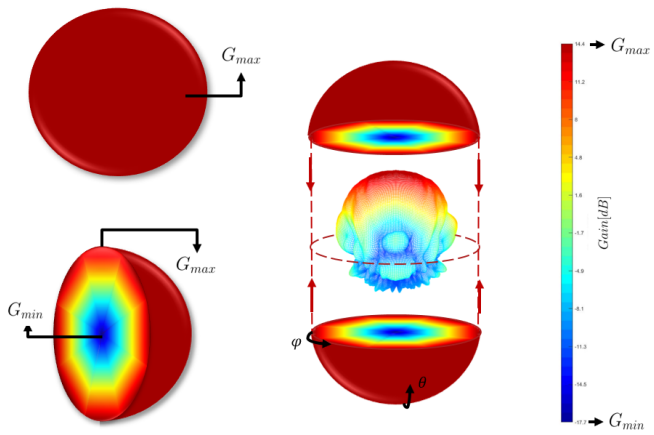

Fig. 13. Coverage function methodology applied to the 17-entry codebook envelope of the PBS array.

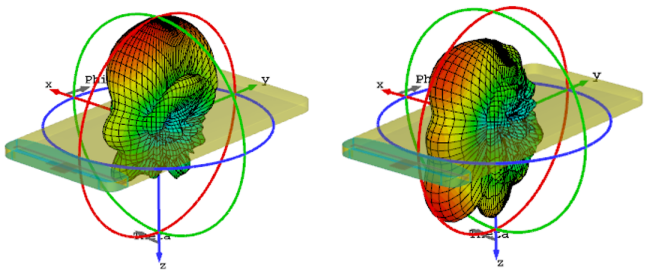

(a) (b)

Fig. 14. CST's point density; a) PBS in the form factor; b) MBS in the form factor.

$$pc_w(\theta) = \frac{\sin\theta d\theta d\phi}{4\pi}; \tag{2}$$

This will then create a curve representing the coverage percentage, $Coverage_{\%}$, for L levels of $G_{threshold_l}$.This calculation is described in Equation 3, where $N_{G_{threshold_l}}$ is the number of points that are above $G_{threshold_l}$, pc_w is the corresponding weight value according to the points' θ coordinate and P is the total number of points analyzed.

$$Coverage_{\%} = \frac{\sum_{n=1}^{N_{G_{threshold_l}}} pc_w(\theta_n)}{P}; \tag{3}$$

Figure 15a) displays the coverage curves of the PBS and MBS for the codebooks displayed in Figure 12 , for several values of $G_{threshold}$. This is similar to a CDF representation. The phase shifter has a 5 bit resolution and 360^o range.

For a coverage study comparison, G_{max} takes the form of the highest gain value out of the two codebook envelopes. In this case, $G_{max_{PBS}} = 14.33$ dB and $G_{max_{MBS}} = 14.08$ dB. The curve starts at 100% because all the gain values evaluated will be higher than G_{min}. For smaller values of threshold gain, at the sphere's core, the MBS array has the biggest coverage percentage. To cover 50% of the analyzed solid angle values, the PBS has to forfeit $G_{max} - G_{Threshold|50\%} = 14.84$ dB, while the MBS would have to forfeit, under the same

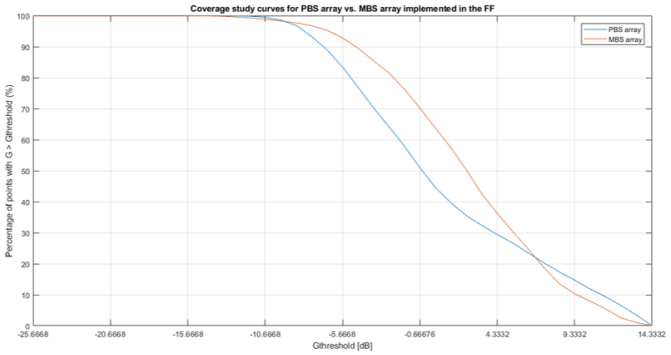

(a)

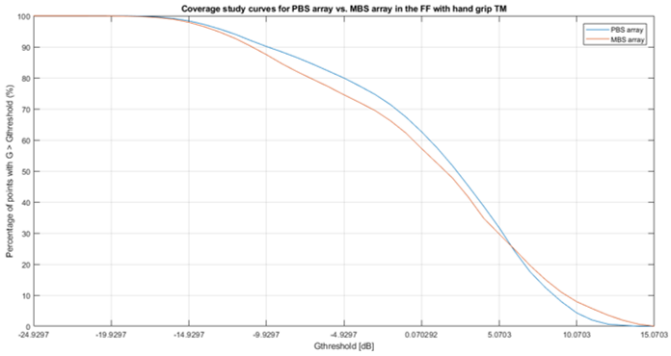

(b)

Fig. 15. Coverage study curves for PBS vs. MBS implemented in the form factor; a) Free space; b) With TM hand grip.

principle, 11.96 dB. This is because, despite having similar maximum gain values, the MBS array has a wider codebook envelope shape, that extends in all directions. The PBS, on the other hand, radiates in a slightly more concentrated number of directions, which explains that, when the threshold value passes the curves' crossing point, the PBS takes the lead. This reiterates the delicate balance between coverage and gain.

These tests were repeated to include the TM hand grip, in order to account for the user's body blockage effect. Figure 15 b) shows that adding in the user's hand makes the coverage curves get even closer to each other. This happens because, as seen above, the hand alters the radiation patterns, rendering them to a random shape with a certain gain value. This further validates the hypothesis that there is really no difference in using PBS and MBS when all environment components are taken into account and, therefore, fabrication and cost considerations will prevail.

V. MIMO CHANNEL SIMULATOR

A 3D geometric discrete scattering channel model was implemented to recreate any type of scenario for mm-Wave propagation. It uses realistic antenna characteristics and also the studies made above regarding form factor influence, beamforming, user inherent body blockage and user induced phone rotation. It will be used to determine the channel's performance for each antenna type when the UE is subjected to different environment scenarios, orientations in space and hand grips.

A. Channel model

The channel model was idealized for a hybrid MIMO + BF scenario, like the one in Figure 16. The UE has two arrays in the bottom back of the phone, A_{UE1} and A_{UE2}, and two arrays in the BS, A_{BS1} and A_{BS2}. The two pairs of arrays create four individual transmission paths, each one of them with a complex transmission coefficients, h_{11}, h_{12}, h_{21} and h_{22}. Once put together, these coefficients form a 2x2 channel matrix H that summarizes in matrix form the current channel state in response to the environment.

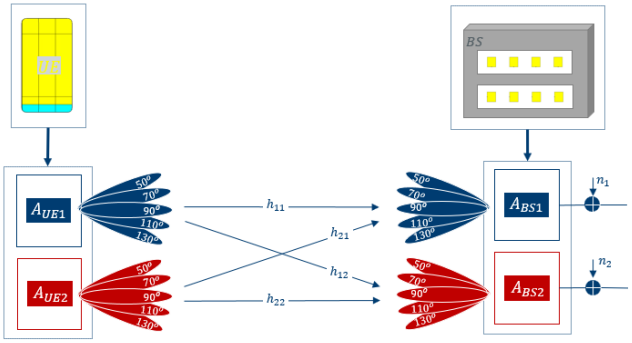

Fig. 16. Schematic view of idealized MIMO + BF system for the simulator.

The BS's arrays, A_{BS1} and A_{BS2}, spaced by a 2.5 cm gap, are two linear, four element PBS arrays with orthogonal polarizations, one over x axis, and another over the y axis. The UE's two arrays, A_{UE1} and A_{UE2}, are integrated in the back of the phone. These can be either PBS or MBS arrays.

If PBS is to be considered, the two arrays consist of one dual polarized PBS array, where spatial multiplexing is performed. It is a 2x2 MIMO + BF transmission mode. However, for the MBS family, the two arrays are placed symmetrically in the mobile phone, horizontally and with the same orientation due to lack of space for a orthogonal polarization arrangement. Because of this, two transmission modes are anticipated. In a predominantly LOS environment, the chosen mode will potentially be a SISO + BF transmission mode. On the other hand, in an environment with enough reflections, the transmission mode will be, similarly to the PBS, a 2x2 MIMO + BF transmission mode.

The number of beams generated has been set to five codebook entries, $b = 5$. These are $\psi = 50^o$, $\psi = 70^o$, $\psi = 90^o$, $\psi = 110^o$, $\psi = 130^o$. As an example, the UE and BS are separated by a distance $d_{LOS_{UE,BS}} = 120$ m and, between them, $S = 15$ obstacles are distributed randomly over a confined space. These scatterers mimic every day obstacles in an urban area and move randomly along the x axis over time. Moreover, they induce a Gaussian distributed polarization rotation, being responsible for creating enough reflections of the signal (multipath) to allow for the MIMO channel to be successfully created.

Therefore, the H matrix will be created for a specific set of environment conditions during a large number T of time slots, in order to create a fading distribution that can be evaluated. Because all beam combinations between the BS

array and the UE array, C, will be taken into consideration, the H matrix will be calculated $T \times C$ times, thus becoming a 3-dimensional matrix with dimensions $b \times b \times C$, from which a beam selection algorithm will by applied to chose the right combination. The resulting H matrix will then be put through the channel assessment metrics that will decide on the channel's performance for a specific antenna family.

B. H matrix calculation

In a typical urban environment there are two signal propagation types. On one hand, there is the direct line of sight path (LOS), when the transmitter and the receiver have an unobstructed path between them. On the other hand, there is also propagation through multipath (MP), where the signal is reflected and scattered into multiple directions only to arrive at the receiver trough several different paths and and with different phase shifts. So, in order to obtain the channel state matrix, both types of components must be recreated in the simulator and considered into the calculations, as seen in Equation 4.

$$H = H_{LOS} + H_{MP}; \tag{4}$$

C. Phone rotation

While using the phone, the user will unwillingly change its orientation relative to the base station. By rotating the phone, the UE's original polarization might change and not match the BS's polarization anymore, which might result in a loss of signal, affecting the MIMO channel's performance.

Therefore, in order to grasp the full effect of UE rotation in the MIMO channel, it is important to observe the rotation in all 3 axis, x, y and z. CST's farfield plot properties allow for LCS selection (also called Working Coordinate System in CST, or WCS) for radiation pattern observation. Using one radiation pattern calculation, it is possible to mimic another phone position with respect to the reference axis frame to extract the corresponding E-field data to use in the simulator for the H matrix construction.

A total of 18 phone positions were chosen, separated by a 45^o rotation motion in all three axis, as seen in Figure 17a). These positions are meant to represent the range of motion of the mobile phone, both for the phone alone and the phone with the user's hand included, as can be seen from Figure 17b).

D. Array coupling

Another influencing factor on the MIMO channel performance is the array coupling between arrays in the same device. If the coupling between the two arrays is high that means that the arrays are too close and there's energy waste that could be applied into transmitting the signals. Also, if part of an array's energy goes into the other array, some of its information gets misdirected, originating cross-talk. In order to account for this correctly in the model, the array's feeding network must be defined, so that each array is represented by one single port using CST's circuit analysis tool, as seen in Figure 18. This will return a 2×2 S-parameters matrix that will allow to calculate the channel's transmission matrix T, Equation 4, that quantifies the amount of existing crosstalk.

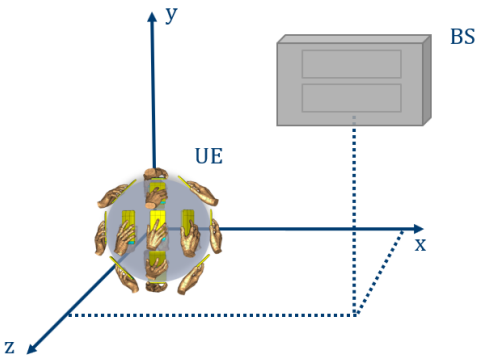

(a)

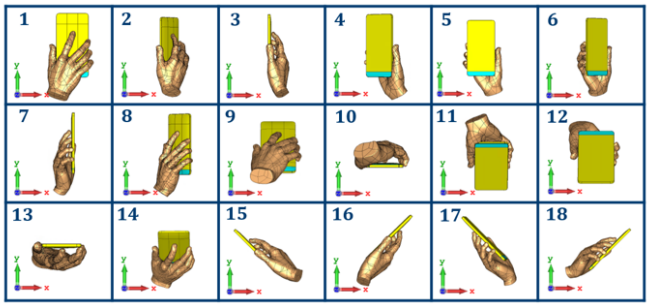

(b)

Fig. 17. Introducing phone rotation into the system; a) 3D representation of the rotation modes; b) Notation for the 18 rotation positions.

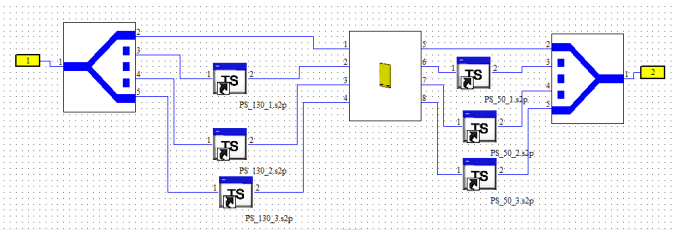

Fig. 18. CS schematic view of the circuitry used for obtaining the array coupling values between the UE's MBS arrays for the beams $\psi_{A1} = 130$ and $\psi_{A2} = 50$.

$$[T] = \begin{bmatrix} \sqrt{1 - s_{11}^2} & s_{12} \\ s_{21} & \sqrt{1 - s_{22}^2} \end{bmatrix} \tag{5}$$

Simulations showed that for the PBS and MBS array placement used in this work, the diagonals of the T matriz came very close to one and the cross talk entries were close to 0 (in linear units). This means that there was no significant array coupling to account for in the H matrix.

E. Beam pair link selection

The beam pair selection criteria varies according to the MIMO approach. If it is SISO, a received power metric is enough. By analyzing the channel's power matrices, as seen in Figure 19, the entry with the highest power is chosen. However if MIMO is in vigor, this received power criteria is accompanied by a condition number metric (CN). CN is an

indicator of MIMO quality and it should be as close to 1 as possible for ideal MIMO communications. If $CN > 10$, then MIMO is not possible and SISO is the only alternative.

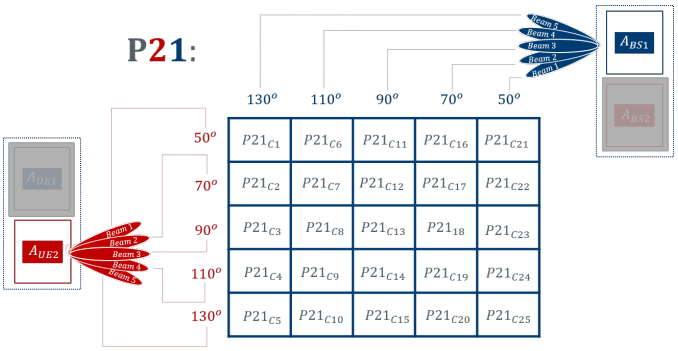

Fig. 19. P21, a particular power matrix for the h_{21} channel.

F. MIMO channel capacity

The channel capacity is the main metric chosen to evaluate the MIMO channel performance. Equation 6 expresses Shannon's capacity theorem. N_r and N_t represent, respectively, the number of transmitting and receiving arrays of the system, while I_{Nr} is a $N_r \times N_r$ identity matrix, H_n is the normalized channel matrix of the system, and SNR is the receiver's signal to noise ratio.

$$C = log_2(det\ [I_{Nr} + \frac{SNR}{N_t} H_n H_n^H])\ bit/s/Hz; \quad (6)$$

It is important to mention that this calculation of C is the best case scenario value of capacity, since it only takes into consideration the channel conditions and considers processes such as modulation/demodulation and coding/decoding of the signal to be ideal.

Although Equation 6 can be applied for both MIMO and SISO channel capacity, the parameters used differ. For a 2×2 MIMO scenario, N_t=N_r=2 and H is a 2×2 matrix. For a SISO scenario, N_t=N_r=1 and H matrix is reduced to a single h element.

Regarding the SNR calculation, many MIMO models fix this metric at a reasonable value, generally 10 to 20 dB. However in this simulator the SNR is calculated over time using a link power budget and is susceptible to the environment characteristics and distance between the antennas.

VI. MIMO Channel Performance Evaluation

A. MBS transmission technique

The choice of using either SISO or MIMO with the MBS must be made using the CN metric. If CN is higher than 10, in linear units, this means that MIMO can't be properly performed and the MBS would then change its transmission scheme from MIMO to SISO.

Table I list the CN values, as well as the SISO capacity and MIMO capacity for all 18 UE positions in LOS.

As expected, for CN values below 10, MIMO increases the channel capacity when compared to SISO. However, surprisingly, for very high CN values, such as in positions 5, 9, 10 or 11, the MIMO capacity values don't stray too far from the SISO capacity. This shows that there is no advantage in implementing SISO in the phone as a transmission technique, since MIMO will always provide a better channel capacity and potentially deteriorating into SISO, but never below that. Therefore, from now on, the transmission technique considered for the MBS will the the same as the PBS, 2×2 MIMO.

TABLE I
LOS channel metrics for MBS SISO vs MIMO

LOS Position	CN	Capacity	
		SISO	MIMO
1	13.4	6.10	7.02
2	2.93	6.38	10.02
3	4.21	6.24	7.20
4	3.68	5.97	8.35
5	36.7	7.34	7.94
6	8.52	6.93	8.56
7	4.43	6.66	7.02
8	7.62	6.77	8.97
9	344.7	9.27	9.45
10	226.1	8.01	7.96
11	61.51	9.94	10.31
12	6.54	5.07	6.73
13	19.82	3.62	3.49
14	6.28	3.42	3.53
15	4.93	5.99	7.62
16	3.69	5.61	6.95
17	2.34	7.41	11.96
18	2.27	6.98	11.37

B. MIMO channel performance sensitivity to phone rotation

The channel metrics for all 18 positions will be evaluated for numerous test scenarios such as (Line-of-Sight) LOS, LOS + Multipath (MP) and (No Line-of-Sight) NLOS + MP with addition of the user's hand influence in TM, which will provide the simulations with the maximum achievable level of realism for the test scenarios:

- LOS: reference scenario where there is solely the unobstructed direct path without any source of multipath.
- LOS with MP: The scatterers within the scatterer rectangular limit will increase the multipath needed to create a multipath-rich MIMO channel.
- NLOS: For this scenario, the LOS component is expected to be almost null, due to the obstruction of the line-of-sight path between the UE and the BS by an obstacle. However, adding MP to the environment would give the signal alternative paths to the one that is blocked and communications would be possible again.

These will be used to create CDF curves that translate the MIMO channel's capacity distribution over the phone's rotation positions. From the three environments tested, the one that presented the highest data rate values was the LOS + MP, Figure 20 b), followed by NLOS + MP, Figure 20 c), and finally, LOS Figure 20 a). These results confirm that the presence of scatterers in the environment result in an increased MIMO channel performance. This is because MIMO strives in MP rich environments, since there are multiple paths created for the signals to propagate through.

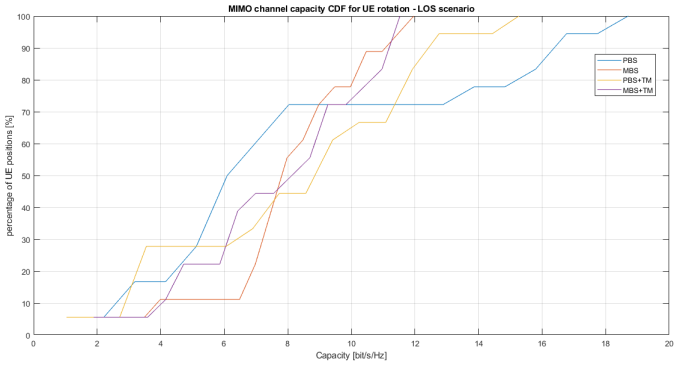

(a)

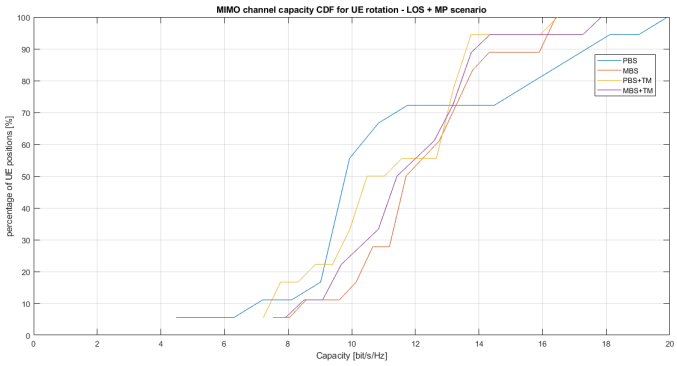

(b)

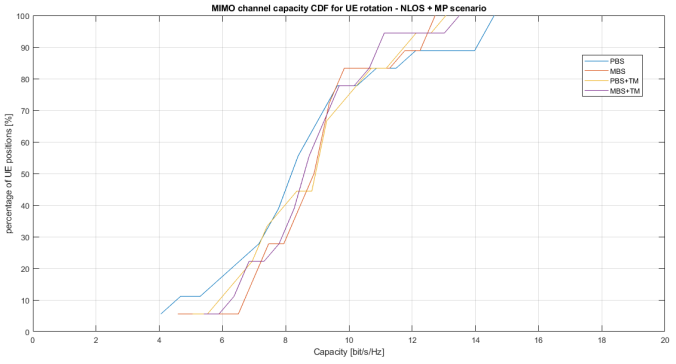

(c)

Fig. 20. Capacity CDF according to the UE positions for PBS, MBS, PBS + TM and MBS+TM; a) LOS b) LOS + MP; C) NLOS + MP; a) LOS; b) LOS + MP; NLOS + MP.

Moreover, by evaluating the median values of these channel capacity distribution over over the UE orientation, it is possible to conclude that, despite the MBS performing a little better than the PBS, the results aren't so different, especially when considering the hang grip influence. This reveals, once more that, in realistic environment conditions, it is indifferent to use PBS or MBS from a MIMO performance standpoint.

VII. Conclusions

In conclusion, the two stage comparison process between the PBS and MBS reveals that, despite the MBS being the winner, both antenna solutions are actually quite similar when it comes to gain coverage and MIMO channel performance, especially when adding the effect of the hand grip into the simulations. It was discussed already that the MBS is a smaller, easier to implement, less complex and cheaper solution when compared to the PBS.

The Occam's razor is a principle of problem solving that states that the correct answer tends to the the simplest one. In that sense, between the PBS and MBS, the MBS seems to be the answer to the problem of mm-Wave antenna implementation in 5G smartphones.

The study also shows that, despite the meager space available in the phone, mm-Wave arrays can still be added and bring the MIMO capacity enhancement to the mobile phone. Nevertheless, more arrays would be needed in the UE in order to improve coverage for all possible rotations and hand grips, using an appropriate switching scheme.

VIII. Acknowledgments

This work was conducted at Intel Mobile Communications in Aalborg, Denmark with the support of Instituto de Telecomunicações.

References

[1] W. Hong, S. Member, K.-h. Baek, S. Ko, and I. Paper, "Millimeter-Wave 5G Antennas for Smartphones : Overview and Experimental Demonstration," *IEEE Transactions on Antennas and Propagation*, vol. 65, no. 12, pp. 6250–6261, 2017.

[2] W. Hong, K. Baek, Y. Lee, and Y. G. Kim, "Design and analysis of a low-profile 28 GHz beam steering antenna solution for Future 5G cellular applications," in *IEEE MTT-S International Microwave Symposium Digest*, 2014.

[3] Y. Huo, X. Dong, and W. Xu, "5G Cellular User Equipment: From Theory to Practical Hardware Design," *IEEE Access*, vol. 5, pp. 13 992 – 14 010, 2017. [Online]. Available: https://arxiv.org/pdf/1704.02540.pdf

[4] O. Jo, J. J. Kim, J. Yoon, D. Choi, and W. Hong, "Exploitation of Dual-Polarization Diversity for 5G Millimeter-Wave MIMO Beamforming Systems," *IEEE Transactions on Antennas and Propagation*, vol. 65, no. 12, pp. 6646–6655, 2017.

[5] S. Sun, T. S. Rappaport, R. W. Heath, A. Nix, and S. Rangan, "MIMO for millimeter-wave wireless communications: Beamforming, spatial multiplexing, or both?" *IEEE Communications Magazine*, vol. 52, no. 12, pp. 110–121, 2014.

[6] W. Hong, "Solving the 5G Mobile Antenna Puzzle," *IEEE Microwave Magazine*, vol. 18, no. 7, pp. 86 – 102, 2017.

[7] K. Zhao, J. Helander, D. Sjöberg, S. He, T. Bolin, and Z. Ying, "User Body Effect on Phased Array in User Equipment for the 5G mmWave Communication System," *IEEE Antennas and Wireless Propagation Letters*, vol. 16, pp. 864–867, 2017.

[8] T. Wu and C. M. Rappaport, Theodore S., Collins, "Safe for Generations to Come," *IEEE Microwave Magazine*, vol. 16, no. 2, pp. 65–84, 2015.

[9] M. Jensen and J. Wallace, "MIMO wireless channel modeling and experimental characterization," in *Space-Time Processing for MIMO Communications*, 1st ed., A. B. Gershman N. D. Sidiropoulos, Ed. John Wiley & Sons, Ltd, 2005, ch. 1, pp. 1–35. [Online]. Available: http://onlinelibrary.wiley.com/doi/10.1002/0470010045.ch1/pdf

[10] ETSI, "TR 138 901 - V14.0.0 - 5G; Study on channel model for frequencies from 0.5 to 100 GHz (3GPP TR 38.901 version 14.0.0 Release 14)," ETSI, Tech. Rep., 2018. [Online]. Available: http://www.etsi.org/standards-search

[11] Corning, "Corning Gorilla Glass 5 PI Sheet," https://www.corning.com/microsites/csm/gorillaglass/PI_Sheets/Corning%20Gorilla%20 Corning, Tech. Rep., 2016.

[12] D.Andreuccettia and R.Fossi, "Dielectric Properties of Body Tissues in the frequency range 10 Hz - 100 GHz," http://niremf.ifac.cnr.it/tissprop/.